Hyperfine structure of metastable levels in $^{151,153}Eu^+$ by collinear laser-rf double-resonance spectroscopy

A. Sen and W. J. Childs
Argonne National Laboratory, Argonne, Illinois 60439-4843
(Received 6 April 1987)

The laser-rf double-resonance technique has been used to make high-precision measurements of the hyperfine structure of the $4f^7(^8S^0)5d\ ^9D^0_{2,3,4,5}$ metastable levels in $^{151,153}Eu^+$. A new apparatus which uses a collinear laser and a slow ion beam (~ 1.35 keV) enables us to achieve a long transit time in the rf region. Consequently, narrow linewidths of ~ 60 kHz have been observed for the first time in such systems. The magnetic dipole and electric quadrupole hyperfine constants (A and B, respectively) of these metastable levels have been determined with a higher precision (2–3 orders of magnitude) than before. A J-dependent magnetic hyperfine anomaly has been observed in the $^9D^0_J$ states. In addition, more accurate values of nuclear quadrupole moments of the two isotopes $^{151,153}Eu^+$ have been determined.

I. INTRODUCTION

Following the principle of the atomic-beam magnetic-resonance (ABMR) technique[1] and optical-rf double resonance,[2] Rosner *et al.*[3] introduced the laser-rf double-resonance method for high-precision spectroscopy. The method replaces the two conventional inhomogeneous magnetic-field regions of the ABMR by two corresponding regions of resonant laser excitation and the rf-field region is located between the two.

The first application of the laser-rf double-resonance method to atomic ions was demonstrated on Xe^+.[4] Since then only a few different systems (U^+, Ba^+, Kr^+, Er^+) (Refs. 5–8) have been reported in the literature. We report here the first precise measurement of the hyperfine constants A and B for $^{151,153}Eu^+$ in the metastable states $4f^7(^8S^0)5d\ ^9D^0_{2,3,4,5}$ employing this technique. A brief report[9] on the technique used in the Eu^+ measurements has appeared elsewhere.

The choice of the rare-earth ion Eu^+ for the investigation arose in part from the relative purity of the states studied and partly from the ease with which the ions could be produced in their metastable states in an arc-discharge ion source (Colutron). Also, the existence of only two natural odd isotopes of Eu^+ with about equal abundance and differing by two mass units makes the mass resolution and spectral identification much easier.

Although the hyperfine structure of $^{151}Eu^+$ and $^{153}Eu^+$ in the ground state and a few excited states had been measured[10–12] by interferometric methods previously, it was not until the laser-excited fluorescence measurements of Arnesen *et al.*[13] and Dörschel *et al.*[14] that the hyperfine constants A and B were determined with some accuracy. The laser-excited fluorescence of fast ion beams in the collinear geometry takes advantage of kinematic compression[15–17] (which reduces the Doppler width) and high selectivity of excitation by narrow-band lasers and mass-resolved ions, resulting in a high spectral resolution. The typical linewidths are 30–150 MHz. Furthermore, the long laser-ion interaction region in the collinear geometry leads to greater detection efficiency of the fluorescence.

Although the kinematic compression of the fast ion beam reduces the Doppler width in principle, the practical limitation in an experimental situation arises out of the fluctuation of the high-voltage terminal which provides the acceleration of the ions. Arnesen *et al.* reported linewidths of 100–150 MHz at 30–40-keV ion energy. The linewidth with the rf-resonance method is limited only by the transit time of the ions through the radio-frequency region and fast ion beams would mean smaller transit time and broader linewidths.

We have built a collinear laser and ion-beam apparatus where the ions are relatively slow (~ 1.35 keV). It is easy to maintain the terminal acceleration voltage constant with the help of a stabilized power supply. From our measurement of laser-excited fluorescence in Eu^+ the typical linewidths with such slow ion beams are 48–75 MHz, which is better than that typically achieved in the fast-beam machines. Further, in our apparatus the ions have the advantage of spending a longer time (~ 12 μs) in the rf region, which results in a much narrower linewidth. We report here the narrowest linewidths (58–70 kHz) yet seen in a collinear laser-ion apparatus. Other advantages of the new apparatus are its very small size and the much smaller rf power levels required. The reduced rf power requirement results both from the much longer time the slower ions spend in the rf field and from the design of the rf structure itself.

II. EXPERIMENT

A. The method

In order that the laser-rf double resonance can be measured, some preliminary knowledge of the hyperfine spectra of the optical transition is necessary. We first recorded the laser-excited fluorescence spectra of $^{151}Eu^+$ and $^{153}Eu^+$ for all the four metastable levels ($^9D^0_{2,3,4,5}$) and assigned the quantum numbers of the transitions in-

volved and obtained the hyperfine intervals with an uncertainty of a few MHz. This is a prerequisite to high-precision rf-resonance measurement where the uncertainty is three orders of magnitude smaller.

The laser-excited fluorescence uses the Doppler principle. In the reference frame of an ion (atom) moving with a velocity v, the laser frequency (ν_L) appears as

$$\nu_0=\nu_L\frac{1-\beta\cos\theta}{(1-\beta^2)^{1/2}}\ , \tag{1}$$

where $\beta=v/c$, c is the speed of light, and θ is the angle between the direction of the propagation of the laser and the velocity of the ion. For slow ions (small v), β is very small and hence expanding the right-hand side of Eq. (1) and retaining only the first-order terms in β, we obtain

$$\nu_0(\theta=0)=\nu_L(1-\beta)\ , \tag{2}$$

where $\nu_0(\theta=0)$ is the frequency seen by the ions when the laser and the ion propagate in the same direction in the collinear geometry. When $\nu_0(\theta=0)$ equals a transition frequency of the ion in its moving frame of reference, then the laser photon may be resonantly absorbed by the ion resulting in an excitation to a higher level and the subsequent decay to the other levels is recorded as fluorescence. From (2) it is easy to see that the ions can be made to resonantly absorb the laser photon either by tuning the laser frequency or by tuning the velocity of the ion beam. We have chosen to keep the velocity fixed and scan the laser.

In the laser-rf double-resonance method, the pump, the rf, and the probe regions are conventionally designated as the A, C, and B regions, respectively, and are in that order. The A and B regions are identical in construction. The ions are made to resonantly absorb the laser photon in the region A resulting in a transition $F\rightarrow F'$. Since the subsequent decay is not entirely to the initial state, the population of the hyperfine level F is depleted. The level is repopulated to some extent by inducing a transition between the neighboring hyperfine levels $F\pm1\rightarrow F$ by an appropriate rf field in the region C. The degree of repopulation is probed in region B, which is observed as an increased laser-excited fluorescence activity. The rf resonance is observed by scanning the applied rf.

B. The apparatus

The new collinear laser and slow-ion-beam apparatus is shown schematically in Fig. 1. It consists of a Colutron ion source (Colutron Research Corporation, Model 101) where solid Eu metal is introduced in a stainless-steel charge holder and Eu^+ ions are produced in an arc-discharge plasma. Many of these ions are easily formed in the metastable levels such as $4f^7(^8S^0)5d\ ^9D^0_J$. The ions are extracted and accelerated to 1.35 keV using a stabilized power supply (Power Design Inc. Model

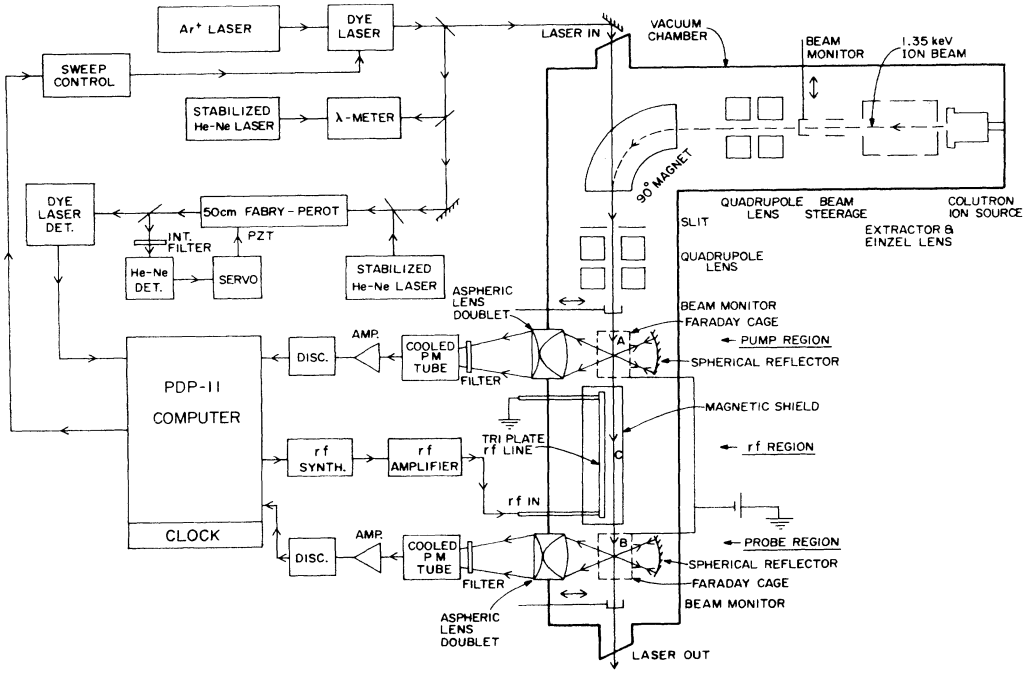

FIG. 1. Schematic diagram of the collinear laser and slow-ion-beam apparatus with computer-controlled data-acquisition system. Ions are produced in a Colutron source, accelerated to 1.35 keV, mass analyzed by a 90° magnet, and move collinearly and parallel to the laser beam over a distance of ~100 cm. The Faraday cages are each 10 cm long and the rf-interaction region is ~50 cm. A cw dye laser pumped by an Ar^+ laser is used. Fluorescence light from the Faraday cages is collected by aspheric-lens optics and spherical reflectors onto cooled photomultiplier tubes and the data processed by a PDP-11 computer or recorded on a chart recorder.

2K-10), focused by an einzel lens and an electrostatic quadrupole lens onto the entrance slit of a 90° magnet. The mass-selected ions emerge from the exit slit of the magnet and are rendered parallel by a second quadrupole lens and enter the interaction region. Light from a dye laser overlaps the ion beam collinearly in the interaction region over a distance of about 1 m.

The interaction region consists of three sections, *A*, *C*, and *B* (as shown in the figure). The pump (*A*) and the probe (*B*) regions, where laser resonance and fluorescence take place, are identical in construction. Each fluorescence region is made of an open-ended, cylindrical, and isolated Faraday cage coaxial with the ion beam and the laser beam, and can be biased to some potential (-100 to -500 V). There are openings on the opposite walls of the Faraday cage for fluorescent light to emerge and the openings are covered by 95% transparent Ni wire mesh (Buckbee-Mears Operation) for electric field definition. Fluorescent light is collected by an aspheric lens doublet and detected by a cooled (-16 °C) photomultiplier tube with an appropriate interference (passband) filter. A spherical reflector is provided for increased light-collection efficiency. The signal from the photomultiplier tube is amplified and discriminated before being sent to a count-rate meter from which the analog signal is sent to a strip-chart recorder.

The radio-frequency region (*C*) is 49.8 cm long and is located between the pump and the probe regions. The rf power is applied at *C* through a tri-plate rf line.[18] The tri-plate rf transmission line consists of a center strip of metal of appropriate width and thickness placed symmetrically between two ground plates. The rf power is applied at one end of the center strip. The ion beam passes between the center strip and one ground plate and interacts with the rf magnetic field. The advantage of such a transmission line is the requirement of low rf power. A heat-treated Permalloy magnetic shield (which also serves as ground planes) is provided to reduce any Zeeman broadening. The rf power is provided by a frequency synthesizer (Rockland Model 5100) and a signal generator (Systorn Donner Model 1702), amplified by different rf amplifiers [Mini-Circuits Model ZHL-42 (SMA), Hewlett Packard 8349A Microwave Amplifier and other homemade amplifiers] and controlled by a PDP-11 computer. A frequency doubler (Hewlett Packard Model 11721A) is sometimes used for the appropriate frequencies and amplification. Typical rf power level used is 0.02–0.08 W.

The laser light is obtained from a tunable single-mode dye laser (Coherent 599-21) driven by an Ar^+ ion laser (Coherent Cr-12). The wavelength is measured by a traveling-arm Michelson λ meter. The laser, the rf source and the output of the photomultiplier tube are handled by computer control using standard electronics.

The apparatus is pumped by two diffusion pumps and an ion pump. The operating pressure in the interaction region is 1×10^{-6} torr. There are several beam monitors and steerage systems along the ion path for measurement of ion current. The fluorescence regions are coated with Aquadag and provided with light baffles for minimizing scattered light.

C. Procedure

A mass-selected ion beam of Eu^+ is easily obtained in the interaction region and the mass spectrum shows very good mass resolution of $^{151}Eu^+$ and $^{153}Eu^+$. Typical ion-beam intensity at this point is $\sim$50–90 nA (per isotope) and the laser intensity is 20–40 mW. The laser system, the ion source and the magnet come to a stable operating condition within about $\frac{1}{2}$ hour of running.

For recording the laser-excited fluorescence spectrum only the region *A* is used. The Faraday cage is biased to a convenient potential (-100 to -300 V) where the ions are accelerated further. Keeping the Faraday-cup voltage fixed, the laser is scanned to bring it into resonance with an optical transition frequency $F\rightarrow F'$, where the ions are excited to the upper level F'. This resonance is recorded by the fluorescence to the lower levels. By scanning the laser over a frequency region the entire fluorescence spectrum is obtained.

The laser and the ion beam are superimposed on one another over a distance of about 10 cm in the Faraday cage and the fluorescence signal is collected from a 3.5-cm-long region. Outside the Faraday cage the ions are not affected by the laser (even though they overlap) because of the different Doppler shift, and typically they are off resonance by $\sim$2.5 GHz.

For the laser-rf double-resonance measurements the Faraday cage at *A* is first connected to ground potential and *B* is connected to some potential (typically -100 V). The laser frequency is tuned into resonance with a single hyperfine component $F\rightarrow F'$ (these quantum numbers have been identified from the fluorescence spectrum), which is observed as a fluorescence peak in the photomultiplier tube at *B*. The ions see the laser at *B* only. The cage at *A* is now biased to the same potential as *B*, whereby the fluorescence signal at *B* decreases. This is because the ions now see the laser at *A* also and therefore the particular lower hyperfine level *F* gets depleted (because of the transition $F\rightarrow F'$). This optical pumping affects only the chosen hyperfine level *F* and leaves others undisturbed. In our apparatus, a 1.45-keV $^{151}Eu^+$ ion beam spends about 2 μs in the laser field which gives rise to 20–70 % depletion of the level *F*.

At this point the rf power is applied at *C*. Here the ions are back to their normal velocity. A 1.35-keV $^{151}Eu^+$ ion beam spends about 12 μs in the entire length of the rf region. This, for a resonance frequency of 1 GHz as an example, amounts to 12 000 oscillations of the rf field which gives considerable chance for the ions to interact with the rf field. (Typical hyperfine intervals measured range in frequency from 100 MHz to a few GHz). If the radio-frequency matches the interval between the depleted hyperfine level (*F*) and an adjacent level ($F\pm1$) of the same hyperfine multiplet, the depleted level will be repopulated to some extent following the magnetic dipole hyperfine selection rule $\Delta F=0,\pm1$. This recovered population of level *F* in the region *C* will be displayed as an increase in the fluorescence strength at *B*.

In an actual experiment, the rf field is scanned over a short frequency interval around the resonance position

predicted from laser-excited fluorescence measurement. As the rf is scanned, the rf detuning from resonance as a function of the fluorescence observed at B gives directly the rf transit-time-limited line shape. The radio frequency for resonance is observed to be independent of the Doppler tuning (Faraday cage) voltage V over a range of several hundred volts around the value $V=-100$ V typically used in making measurements.

The resonance frequency is Doppler shifted depending on the relative motion of the rf field and the ion beam. In our apparatus, the rf field propagating along and against the ion beam gives rise to two resonance peaks which are red and blue shifted from the actual frequency as discussed below. The average of the two peak positions gives the required frequency of transition.

III. RESULTS

A partial energy-level diagram of Eu^+ is shown in Fig. 2, where the laser-excited optical transitions from the metastable levels are indicated by upward arrows and the fluorescence to the ground levels is indicated by downward arrows. The hyperfine multiplet structure of the two optical levels $4f^7(^8S^0)4d\ ^9D_2^0$ and $4f^7(^8S^0_{7/2})6p_{3/2}$, $J'=3$ for $^{151}Eu^+$ are shown in Fig. 3. The hyperfine intervals of the level $^9D_2^0$ as measured by rf resonance are indicated in the figure.

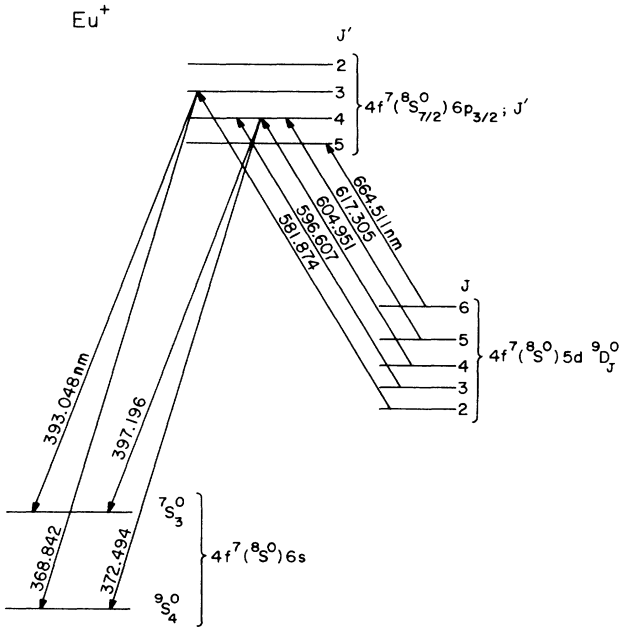

FIG. 2. Partial energy-level diagram of Eu^+ without the hyperfine levels, showing the ground state and a few excited states of the ion. The electron configuration of the states is also indicated. The ground state and the metastable states belong to the LS-coupled scheme whereas the excited states are in the jj-coupled scheme. The resonant laser excitations of the metastable $^9D_J^0$ levels are shown by upward arrows and the fluorescence from the upper levels are shown by downward arrows. The transition wavelengths are given in nm.

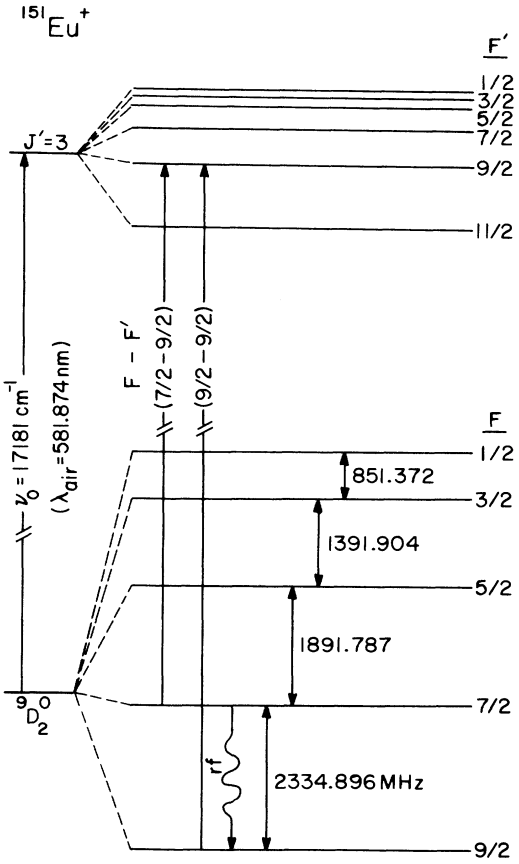

FIG. 3. Hyperfine levels of the metastable $4f^7(^8S^0)5d\ ^9D_2^0$ state and the excited state $4f^7(^8S^0_{7/2})6p_{3/2}$, $J'=3$. The nominal optical frequency between $J=2$ and $J'=3$ is 17 181 cm^{-1}. The lower and the upper states split into $(2J+1)$ and $(2J'+1)$ hf levels, respectively, and the F values are indicated on the right. An example of hf transitions from $F=9/2$ and $F=7/2$ of the lower state to one particular level ($F'=9/2$) of the upper state are shown, the difference of which gives the hf interval between the two lower levels. This is determined from the laser-excited fluorescence spectra (see Fig. 4) to an accuracy of a few MHz. The same interval is determined with a much higher precision to a few kHz by rf double resonance (see text). The hf intervals of the lower state thus determined are given in the figure.

Typical laser-excited fluorescence spectra for $^{151}Eu^+$ and $^{153}Eu^+$ in the metastable state $4f^7(^8S^0)5d\ ^9D_2^0$ excited by laser light ($\lambda=581.874$ nm) to the level $4f^7(^8S^0_{7/2})6p_{3/2}$, $J'=3$, which decay ($\lambda=393.0$ nm) to the $4f^7(^8S^0)6s\ ^7S_3^0$, are shown in Fig. 4. The components are adequately resolved for the purpose of identification and assignment of the transitions which are also indicated in the figure. Such spectra for each isotope and for the four metastable states $^9D^0_{2,3,4,5}$ have been recorded. The observed linewidths are typically in the range 50–80 MHz although the widths shown in Fig. 4 are somewhat larger. The observation and identification of the spectral lines are necessary prerequisities to the next step of high-precision laser-rf

double-resonance spectroscopy.

A typical laser-rf double-resonance spectrum for the interval $F=\frac{9}{2}\leftrightarrow F=\frac{7}{2}$ in the $^9D_2^0$ state of $^{151}Eu^+$ is shown in Fig. 5. This interval is indicated in Figs. 3 and 4. The two rf-resonance peaks are due to the independent interaction of the forward and the reflected rf waves propagating along the shorted 50-Ω tri-plate line with the ion beam.

As mentioned earlier, these two peaks are Doppler shifted in opposite directions and the average of the two peak positions gives the true resonance frequency. The separation of the peaks (equal to two times the Doppler shift) is proportional to the resonance frequency and is consistent with the known ion velocity in the rf region. A Lorentzian fit of each individual peak is shown as the solid line in the figure. The linewidth in this particular case is 58.7 kHz.

In analyzing the hyperfine spectra, we have used only the magnetic dipole and the electric quadrupole interaction terms (despite the high experimental precision, uncertainties in the second-order hfs corrections are large enough that one cannot reliably evaluate magnetic octupole hfs effects) in the hfs Hamiltonian[19,20] given by

$$H_{\rm hfs}=hA\,\mathbf{I}\cdot\mathbf{J}+hB\left[\frac{(3/2)\mathbf{I}\cdot\mathbf{J}(2\mathbf{I}\cdot\mathbf{J}+1)-I(I+1)J(J+1)}{2I(2I-1)J(2J-1)}\right], \tag{3}$$

where

$$\mathbf{I}+\mathbf{J}=\mathbf{F} \tag{4}$$

and

$$\mathbf{I}\cdot\mathbf{J}=[F(F+1)-I(I+1)-J(J+1)]/2\ . \tag{5}$$

Here A and B are the magnetic dipole and electric quadrupole hyperfine constants respectively, I, J, and F are the nuclear spin, electronic, and total angular momentum quantum numbers, respectively, and h is Planck constant.

Each of the upper and lower levels splits into $2J+1$ levels when $I\geq J$, or $2I+1$ levels when $J\geq I$. With $I=\frac{5}{2}$ for Eu^+, the lower metastable level $^9D_2^0$ splits into five sublevels and the upper level with $J'=3$ splits into six sublevels (see Fig. 3). Using proper selection rules, a theoretical hf spectrum is constructed involving the A's and B's of the upper and lower levels. A good agreement is obtained with the experimental laser-excited fluorescence spectrum in each case. The hyperfine intervals of the lower levels are expressed in terms of the cor-

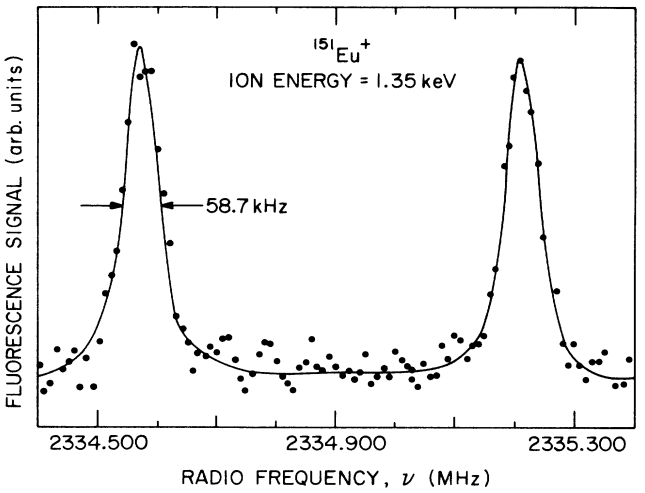

FIG. 5. Typical laser-rf double-resonance spectrum for the transition $F=7/2\leftrightarrow F=9/2$ in the lower optical state $^9D_2^0$ (see Fig. 3). The two peaks correspond to the interaction of the ion beam with the parallel and counterparallel traveling rf waves resulting in equal but opposite Doppler shifts. The true resonance frequency is taken as the average of the two peak positions. The solid line is a Lorentzian fit of the data points and the linewidth obtained from the fit is 58.7 kHz which is consistent with the ion-transit time of ~ 12 μs in the rf region.

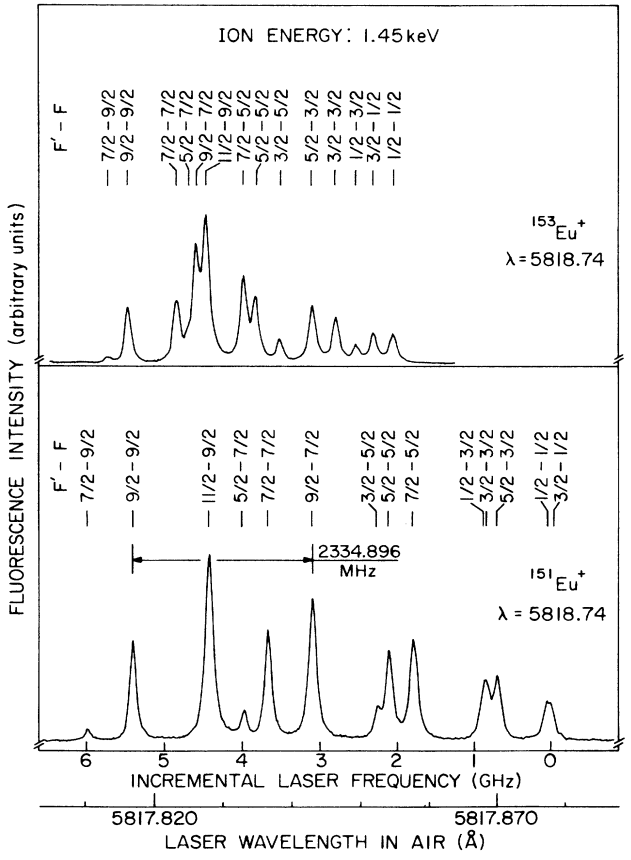

FIG. 4. Typical laser-excited fluorescence spectra for the hf transitions between states $^9D_2^0$ and $6p_{3/2}$, $J'=3$. The upper spectrum corresponds to $^{153}Eu^+$ and the lower one to $^{151}Eu^+$. The ion energy in each case is 1.45 keV. The upper-state (F') and the lower-state (F) values of the F quantum numbers are indicated above each transition. Most of the peaks are resolved even though the linewidths are ~ 100 MHz in these spectra. Narrower linewidths (50–75 MHz) have been observed in other spectra with our apparatus.

responding A's and B's and their values are obtained from making a least-squares fit to the intervals determined from laser-rf double-resonance measurements.

The hf intervals for the lower metastable levels $^9D^0_{2,3,4,5}$ for both the isotopes of Eu^+ measured with the double-resonance technique are given in Table I. The A and B values obtained from least-squares fitting the observed intervals are given in column 3 of Table II. The hf intervals calculated with the fitted values of A and B and their departure from the measured values are also given in Table I. The values obtained by Arnesen *et al.* (1981) are also given in Table II for comparison.

Using the experimental intervals, the A and B factors are determined by a least-squares-fitting procedure. The calculated hf intervals showed some departure from the experimental values which was suspected as due to

TABLE I. Hyperfine intervals of the $4f^7(^8S^0)5d\ ^9D^0_{2,3,4,5}$ states of $^{151}Eu^+$ and $^{153}Eu^+$ from laser-rf double-resonance measurements. Using the experimental intervals of column 4, second-order corrections to the energy were calculated and the corrected intervals are given in column 5. The A and B constants are determined from a least-squares fitting of the corrected intervals. The calculated intervals in column 6 are in very good agreement with those in column 5 as can be seen from the small residuals in column 7.

State and excitation energy (cm^{-1})	Mass No.	Transition $F+1$-F	Expt. hf interval[a] (MHz)	corrected hf interval (MHz)	Calc. hf interval (MHz)	Difference (MHz)
$4f^75d\ ^9D^0_2$	151	9/2-7/2	(−)2334.496(3)	(−)2335.070	−2335.070	0.000
		7/2-5/2	(−)1891.787(3)	(−)1891.668	−1891.669	−0.001
(9923.00)		5/2-3/2	(−)1391.904(4)	(−)1391.642	−1391.641	+0.001
		3/2-1/2			−851.164	
	153	9/2-7/2	(−)881.247(2)	(−)881.341	−881.336	+0.005
		7/2-5/2	(−)878.057(2)	(−)878.086	−878.094	−0.008
		5/2-3/2	(−)730.443(3)	(−)730.385	−730.395	−0.010
		3/2-1/2	(−)479.619(3)	(−)479.532	−479.511	+0.021
$4f^75d\ ^9D^0_3$	151	11/2-9/2	(−)1379.138(3)	(−)1378.691	−1378.694	−0.003
		9/2-7/2	(−)1018.455(3)	(−)1018.209	−1018.203	+0.006
(10081.65)		7/2-5/2	(−)723.632(4)	(−)723.605	−723.603	+0.002
		5/2-3/2	(−)480.140(4)	(−)480.251	−480.253	−0.002
		3/2-1/2	(−)273.371(5)	(−)273.503	−273.509	−0.006
	153	11/2-9/2	(−)895.135(4)	(−)895.094	−895.094	0.000
		9/2-7/2	(−)452.245(4)	(−)452.130	−452.129	+0.001
		7/2-5/2	(−)177.360(5)	(−)177.296	−177.297	−0.001
		5/2-3/2			−33.234	
		3/2-1/2			+17.423	
$4f^75d\ ^9D^0_4$	151	13/2-11/2	(−)840.522(3)	(−)840.178	−840.157	+0.021
		11/2-9/2	(−)635.067(3)	(−)634.932	−634.937	−0.005
(10312.82)		9/2-7/2	(−)467.684(4)	(−)467.688	−467.700	−0.012
		7/2-5/2	(−)331.451(4)	(−)331.528	−331.539	−0.011
		5/2-3/2	(−)219.445(5)	(−)219.541	−219.549	−0.008
	153	13/2-11/2	(−)595.021(3)	(−)594.926	−594.926	0.000
		11/2-9/2	(−)309.596(2)	(−)309.549	−309.549	0.000
		9/2-7/2			−121.097	
		7/2-5/2			−11.947	
		5/2-3/2			+35.523	
$4f^75d\ ^9D^0_5$	151	15/2-13/2	(−)529.051(2)	(−)528.865	−528.864	+0.001
		13/2-11/2	(−)464.306(2)	(−)464.253	−464.254	−0.001
(10643.48)		11/2-9/2	(−)397.097(3)	(−)397.115	−397.113	+0.002
		9/2-7/2	(−)327.780(5)	(−)327.827	−327.831	−0.004
		7/2-5/2	(−)256.747(5)	(−)256.800	−256.797	+0.003
	153	15/2-13/2	(−)218.052(5)	(−)217.973	−217.972	+0.001
		13/2-11/2	(−)204.019(5)	(−)204.016	−204.018	−0.002
		11/2-9/2	(−)183.570(5)	(−)183.590	−183.589	+0.001
		9/2-7/2			−157.680	
		7/2-5/2			−127.289	

[a]The negative signs of the hyperfine intervals are determined from the laser-excited fluorescence results. This is due to the "inverted" nature of the levels which arises from the fact that the magnetic dipole moments of $^{151}Eu^+$ and $^{153}Eu^+$ are negative.

TABLE II. Hyperfine constants A and B for the $4f^7(^8S^0)5d\ ^9D^0_{2,3,4,5}$ states of $^{151}Eu^+$ and $^{153}Eu^+$ from laser-rf double-resonance measurements. The values are obtained by least-squares fitting of the experimental and corrected hyperfine intervals of Table I. The "corrected" values in columns 4 and 6 follow from applying corrections for second-order hfs to the "experiment" values in columns 3 and 5.

Mass No.	State	A_{expt} (MHz)	A_{corr} (MHz)	B_{expt} (MHz)	B_{corr} (MHz)	Reference
151	$^9D^0_2$	−535.103(3)	−535.084	+ 108.260(25)	+107.863	a
		−540.0(1.8)		+ 108(22)		b
	$^9D^0_3$	−226.307(8)	−226.267	−244.534(91)	−244.044	a
		−228.2(1.6)		−222(20)		b
	$^9D^0_4$	−113.159(1)	−113.141	−215.356(10)	−214.851	a
		−115.3(0.8)		−203(17)		b
	$^9D^0_5$	−71.689(2)	−71.683	+ 19.179(22)	+19.467	a
		−72.0(1.0)		+ 18(23)		b
153	$^9D^0_2$	−237.122(8)	−237.126	+ 275.291(55)	+275.158	a
		−239.7(4.8)		+ 282(41)		b
	$^9D^0_3$	−100.491(6)	−100.473	−622.627(77)	−622.713	a
		−101.8(4.7)		−584(50)		b
	$^9D^0_4$	−50.415(1)	−50.407	−548.357(10)	−548.262	a
		−51.9(3.9)		−547(56)		b
	$^9D^0_5$	−32.051(1)	−32.052	+49.639(24)	+49.809	a
		−32.9(1.2)		+ 72(27)		b

[a]Present work (1987).
[b]Arnesen *et al.* (1981).

higher-order effects. The hf Hamiltonian is not diagonal in J, and this means that the experimental hf intervals have to be corrected for the perturbation by the neighboring J levels. These corrections were computed in the second-order perturbation theory using a computer program *PERJ* and the corrected intervals are shown in Table I. The A and B constants obtained after making these corrections gave much smaller differences between the corrected and calculated hf intervals. Table II lists both the uncorrected (columns 3 and 5) and the corrected (columns 4 and 6) values of A and B. Because the uncertainties in the second-order corrections are difficult to evaluate, the corrected A and B values are given without uncertainties.

IV. ANALYSIS OF hfs

The general theory of hfs was developed by Schwartz[21] (1955) in the relativistic framework in which the hf-interaction Hamiltonian was expressed as a multipole expansion of the electric and magnetic moments. This scheme requires accurate relativistic wave functions which are unwieldy and difficult to obtain. Sandars and Beck[22] (1965) have simplified the problem by introducing the "effective-operator" formalism, in which the nonrelativistic LS-coupled wave functions can be used while retaining the framework of Schwartz's hf Hamiltonian. The effective hf Hamiltonian is given by

$$H^{\text{eff}}_{\text{hfs}} = \sum_k \mathbf{M}^{(k)} \cdot \mathbf{T}^{(k)} , \tag{6}$$

where the $\mathbf{M}^{(k)}$ and $\mathbf{T}^{(k)}$ are spherical tensor operators of rank k for the nuclear and the electronic part, respectively. The terms for $k=1,2,3$, etc., represent the magnetic dipole, electric quadrupole, magnetic octupole interactions, respectively. The wave function for a coupled state is given by $|\alpha IJFM_F\rangle$ where α represents all other quantum numbers needed to specify the state. The hf interaction energy obtained in the first-order perturbation theory is

$$E_{\text{hfs}} = \langle \alpha IJFM_F | H_{\text{hfs}} | \alpha IJFM_F \rangle = \sum_k (-1)^{I+J+F} \begin{Bmatrix} I & J & F \\ J & I & k \end{Bmatrix} \langle I \| M^{(k)} \| I \rangle \langle J \| T^{(k)} \| J \rangle , \tag{7}$$

where $\{\ \}$ is a 6-j symbol and $\langle \|M\| \rangle$ and $\langle \|T\| \rangle$ are the reduced matrix elements of the nuclear and electronic parts of the tensor operators. The expressions for these may be found in the literature.[21,23]

The magnetic dipole and electric quadrupole hf constants are given by

$$A = \mu_N \left[\frac{\mu_I}{I} \right] \frac{\langle J \| T^{(1)} \| J \rangle}{\sqrt{J(J+1)(2J+1)}} , \tag{8}$$

and

$$B = 2eQ \left[\frac{2J(2J-1)}{(2J+1)(2J+2)(2J+3)} \right]^{1/2} \langle J \| T^{(2)} \| J \rangle , \tag{9}$$

where μ_N, and μ_I, and Q are the nuclear Bohr magneton, magnetic dipole moment, and electric quadrupole moment, respectively, and $T^{(1)}$ and $T^{(2)}$ are the electronic part of the magnetic dipole and electric quadrupole operators.[24] Although the angular parts of these matrix elements can be calculated, the radial part has to be evaluated either theoretically or by parametric fitting of the experimentally obtained values of A and B. In this

work we have not attempted to do any theoretical determination of the radial parts. The parametric-fitting approach will be considered next.

A. Parametric fitting

In this approach, the experimentally obtained values of A and B have been expressed in terms of linear combinations of the reduced integrals following the effective-operator formalism of Sandars and Beck. These reduced integrals are treated as free parameters in a least-squares-fitting procedure and their values determined.

The wave functions for the levels $^9D_J^0$ arising from the configuration $4f^7 5d$ in Eu^+ are known[25] to have a high purity in the LS-coupled scheme. For an electron configuration $l^N l'$, the expressions for the matrix elements of the magnetic dipole and electric quadrupole operators are given by Childs[26] (1970). Following this scheme, the A and B constants are expressed as linear combinations of the so-called reduced parameters $a_l^{k_s k_l}$ and $b_l^{k_s k_l}$, where k_s and k_l refer to the rank of the tensors in the spin and the orbital space, respectively. Treating the $^9D_J^0$ levels as pure LS states, the magnetic dipole constants A_J for the $^9D_J^0$ levels are expressed as

$$\begin{aligned}
A_2 &= -\tfrac{2}{3}a_d^{01} - \tfrac{5}{42}a_d^{12} + \tfrac{5}{24}a_d^{10} + \tfrac{35}{24}a_f^{10} , \\
A_3 &= -\tfrac{1}{12}a_d^{01} + \tfrac{19}{336}a_d^{12} + \tfrac{13}{96}a_d^{10} + \tfrac{91}{96}a_f^{10} , \\
A_4 &= \tfrac{3}{20}a_d^{01} + \tfrac{43}{560}a_d^{12} + \tfrac{17}{160}a_d^{10} + \tfrac{119}{160}a_f^{10} , \\
A_5 &= \tfrac{4}{15}a_d^{01} + \tfrac{1}{30}a_d^{12} + \tfrac{11}{120}a_d^{10} + \tfrac{77}{120}a_f^{10} .
\end{aligned} \tag{10}$$

In the nonrelativisitic limit

$$a_l^{01} = a_l^{12} = a_{nl} = 2\mu_B \mu_N \left[\frac{\mu_I}{I}\right] \langle r^{-3} \rangle_{nl} ,$$

where μ_B is the Bohr magneton and $\langle r^{-3} \rangle_{nl}$ is the expectation value of the radial integral, and $a_l^{10} = 0$ for $l, l' \neq 0$. We note in each of the expressions for A_J that the coefficient of the a_f^{10} term is seven times that of the a_d^{10} term. To reduce the number of adjustable parameters, we assume $a_d^{01} = a_d^{12} = a_d$, and we let $7a_f^{10} + a_d^{10} = C$. Thus, the A_J's are expressed in terms of two reduced parameters a_d and C,

$$\begin{aligned}
A_2 &= -0.7857 a_d + 0.2083 C \\
A_3 &= -0.0268 a_d + 0.1354 C \\
A_4 &= 0.2268 a_d + 0.1063 C \\
A_5 &= 0.3 a_d + 0.0917 C .
\end{aligned} \tag{11}$$

Using the corrected values of A_J, the a_d and C parameters for both the isotopes are determined. For $^{15}Eu^+$, $a_{5d} = 254(1)$ MHz and $C = -1613(4)$ MHz. For $^{153}Eu^+$, $a_{5d} = 112.0(5)$ MHz and $C = -716(2)$ MHz.

The quality of this two-parameter fit to the four A values is excellent (the rms residual is only 1.3 MHz). The extremely large value found for C indicates that contact hfs dominates the hyperfine structure. This is completely unexpected since the nominal configuration ($4f^7 5d$) contains no open s shells. It is much too large to arise from the contactlike contributions predicted for the $4f$ and $5d$ electrons by the effective-operator theory. It most likely arises either from core polarization (distortion of inner s shells) or configuration interaction with configurations containing open s shells (such as $4f^7 6s$).

Similar expressions for the B_J are obtained in terms of the b parameter

$$\begin{aligned}
B_2 &= 0.1633 b_d^{02} , \\
B_3 &= -0.3571 b_d^{02} , \\
B_4 &= -0.3377 b_d^{02} .
\end{aligned} \tag{12}$$

Using the corrected values of B_J, the b parameters are determined. For $^{151}Eu^+$, $b_{5d} = 661(6)$ MHz and for $^{153}Eu^+$, $b_{5d} = 1687(15)$ MHz.

B. Hyperfine anomaly

From the expression for A in Eq. (8), it can be seen that for two isotopes 1 and 2, the ratio of the A factors,

$$\frac{A_1}{A_2} = \left[\frac{\mu_1}{I_1}\right] \Big/ \left[\frac{\mu_2}{I_2}\right] = \frac{g_I(1)}{g_I(2)}$$

or

$$\frac{A_1}{A_2}\frac{g_I(2)}{g_I(1)} = 1 , \tag{13}$$

where the g_I's are nuclear g factors. But, in reality, there is a departure from unity in expression (13), which is known as the hyperfine anomaly. Hf anomaly arises due to the fact that the nuclei are not pointlike objects. There is a charge distribution over a finite volume and the nuclear magnetization varies over the extended nucleus.

In the case of Eu^+, $I = \frac{5}{2}$ for both the isotopes ($M = 151$, 153) and the hyperfine anomaly parameter is given by

$$^{151}\Delta^{153} = \frac{A(151)}{A(153)}\frac{\mu_I(153)}{\mu_I(151)} - 1 . \tag{14}$$

The anomaly parameters for the $^9D^0_{2,3,4,5}$ states are given in percent difference in Table III. The value of $\mu_I(153)/\mu_I(151) = 2.265\,05(42)$ is taken from the ground-state measurements[27] in neutral Eu.

It can be seen that there is a definite trend in the hf anomaly in these states, i.e., the anomaly increases in the negative direction with increasing J values. The uncertainties given for the hf anomalies reflect the uncertainties in the experimental A values. Any additional uncertainty due to the second-order corrections is probably much smaller and is ignored.

One cannot attempt even a qualitative analysis of the hf anomaly because of the extreme complexity of the electronic structure (the previously accepted characterization of the electronic configuration $4f^7 5d$ does not even contain a penetrating s electron). The observed hf anomaly gives additional evidence of distortion of inner

TABLE III. Hyperfine anomaly in the $4f^7(^8S^0)5d\ ^9D^0_{2,3,4,5}$ states of $^{151}Eu^+$ and $^{153}Eu^+$. The ratios of the magnetic dipole constants (A), the hyperfine anomaly, and the ratios of the electric quadrupole constants (B) of the two isotopes are given in column 3, 4, and 5, respectively. (See text for explanation.)

State	J	$A(151)/A(153)$	$^{151}\Delta^{153}$ (%)	$B(151)/B(153)$
$4f^75d\ ^9D^0_2$	2	2.2565(1)	−0.377(19)	0.3920
$4f^75d\ ^9D^0_3$	3	2.2520(1)	−0.576(21)	0.3919
$4f^75d\ ^9D^0_4$	4	2.2445(1)	−0.907(19)	0.3919
$4f^75d\ ^9D^0_5$	5	2.2365(1)	−1.260(21)	0.3908
Ground state of Eu I		2.264 98(8)	−0.003(18)	0.3928(20)

shells (core polarization) in these Eu^+ levels which nominally arise from the $4f^75d$ configuration.

Also shown in Table III are the ratios of the B values for the four states as determined from the corrected B values. Because of the unknown size of the uncertainties associated with making the second-order corrections, no uncertainties are quoted for the B-value ratios. It is clear that these ratios are remarkably independent of J. Since nuclear quadrupole moments cannot be precisely measured independent of hfs B values (unlike the situation for the dipole hfs interaction), one cannot directly observe a quadrupole hfs anomaly. We do point out, however, that the independence of the B ratios on J shows that if a quadrupole hf anomaly exists, it is state independent to a high order.

C. Nuclear quadrupole moment and Sternheimer correction

One of the important contributions of measurements of optical hyperfine structure (opt-hfs) is the determination of nuclear quadrupole moments. The method depends heavily on the accurate theoretical knowledge of the electric field gradient at the site of the nucleus, and this gradient is difficult to evaluate. Recently, quadrupole moments have been determined independently and accurately by x-ray spectroscopy of muonic atoms[28] (μ x-ray) or Coulomb excitation[29] (CE) of the nuclei.

In the present work, the radial parameters a_{nl} and b_{nl} have been determined by parametric fitting. The expressions for these are

$$a_{nl}=2\mu_B\mu_N\left[\frac{\mu_I}{I}\right]\langle r^{-3}\rangle_{nl}$$

and

$$b_{nl}=e^2Q\langle r^{-3}\rangle_{nl}\ . \tag{15}$$

Following the simple theory, we assume the radial integrals $\langle r^{-3}\rangle_{nl}$ are the same, and find

$$Q=\left[\frac{2\mu_B\mu_N}{e^2}\right]\left[\frac{\mu_I}{I}\right]\frac{b_{nl}}{a_{nl}}\ . \tag{16}$$

The nuclear magnetic dipole moment (μ_I) can be determined from other separate experiments (for example, from atomic-beam magnetic resonace) accurately, thus providing a way to determine Q from the hfs measurements. But Sternheimer[30] has shown that the nuclear quadrupole moment Q itself causes shielding or polarization of the electron shell and some correction is necessary. The correction (R_{nl}) known as the Sternheimer shielding (or antishielding) factor for the electron in the nl shell, when applied to the apparent quadrupole moment obtained from hfs measurements, gives the true value (Q_{true}) of the quadrupole moment

$$Q_{\text{true}}=Q_{\text{app}}(1-R_{nl})^{-1}\ . \tag{17}$$

The main difficulty in determining Q_{true} lies in accurate determination of the factor R_{nl}. Childs and Cheng[31] have recently determined these R_{nl} factors semiempiri-

TABLE IV. Nuclear quadrupole moments (Q) for $^{151}Eu^+$ and $^{153}Eu^+$. Columns 2 and 3 list the Q values obtained from the optical-hfs measurements without Sternheimer correction. Columns 4 and 5 list the Q values after applying the Sternheimer corrections given in column 7. The two values listed in column 7 are for the two isotopes.

	Uncorrected		Corrected		Electron	Sternheimer correction	
Method	$Q(151)$	$Q(153)$	$Q(151)$	$Q(153)$	shell	R_{5d} used	Reference
Opt-hfs	1.32	3.58	0.94	2.56	5d	−0.4	13
Opt-hfs	1.53(5)	3.92(12)	0.903(10)	2.412(21)	5d	−0.69(6), −0.63(5)	32
Opt-hfs	1.12(6)	2.83(65)			5d		14
Opt-hfs			0.95	2.43	5d	−0.176	33
Opt-hfs			0.95(3)		5d		34
Opt-hfs	1.466(15)	3.741(38)	0.83	2.22	5d	−0.760, −0.685	[a]
μ x ray			0.903(10)	2.412(21)	5d		28
μ x ray				2.50(2)	5d		35
CE				2.50	5d		29
Theory					5d	−0.25(5)	36
Semiempirical					5d	−0.760, −0.685	31

[a]Present work (1987).

cally for a number of rare-earth elements by combining multiconfiguration Dirac-Fock (MCDF) calculations of the radial integrals with the values of Q_{true} determined from CE or μ x-ray methods.

We have determined the apparent values of the nuclear quadrupole moment (Q_{app}) for both the stable isotopes of Eu^+ using Eq. (16) and the values of a_{5d} and b_{5d}, which are given in Table IV. For the nuclear magnetic moments, the values[27] $\mu_I(151)=3.463\,60(6)\mu_N$ and $\mu_I(153)=1.5292(8)\mu_N$ have been used. With semiempirical values of R_{nl} from Childs and Cheng,[31] the true quadrupole moments have been calculated. Also given in the table are the measurements from other references. The Sternheimer corrections for Ref. 32 have been determined from comparing the optical-hfs values with those obtained from μ x-ray methods of Ref. 28.

From the values listed in Table IV it is clear that there is considerable ambiguity in the value of R_{5d}. Tanaka *et al.* have determined R_{5d}, R_{4f}, and R_{6p} values for a number of rare-earth elements and have noted wide variations in the values of R_{5d}, whereas the R_{4f} values are reasonably self-consistent. The R_{6p} values also agree reasonably except for ^{163}Dy. Clearly, more data is needed for a systematic evaluation of the Sternheimer effect.

V. CONCLUSIONS

The conclusions from the present work can be summarized as follows.

(1) The new apparatus, with fullwidth at half maximum (FWHM) of only 60 kHz, makes it possible for the first time to measure hfs splittings in many levels of ions with virtually the same precision routinely achieved in atomic-beam studies of neutral atoms. This greatly facilitates comparison of hfs in different charge states. In addition, the precision makes possible the measurement of quadrupole hfs in atoms with small nuclear electric-quadrupole moments.

(2) The analysis shows clearly that *s*-electron admixture (probably corepolarization) plays a dominant role in the hfs of the $4f^7 5d\ ^9D^0_J$ levels studied. Nielsen[37] has pointed out that the multiconfiguration Dirac-Fock theory, which is the only *ab initio* theory available for calculating hfs in heavy many-electron atoms, has no self-consistent way of taking account of the polarization of these inner shells. The present work emphasizes the importance of further theoretical work on this area.

(3) A clearly *J*-dependent hyperfine anomaly has been observed in the $^9D^0_J$ levels. Because of the complexity of the $4f^7 5d$ electronic configuration, however, no attempt at theoretical interpretation has been made.

(4) Previous atomic-beam efforts to evaluate the nuclear electric-quadrupole moments of ^{151,153}Eu were done in Eu *I*, where the $4f^7 6s^2$ electron configuration is almost exactly spherically symmetric. Because the electric field gradient is almost zero, only rough values could be given for the *Q* values. In the Eu^+, however, the studies are done in the $4f^7 5d$ configuration, and the 5*d* electron provides the needed electric field gradient. Comparison of the results with the muonic x-ray and Coulomb excitation studies give a good value for the Sternheimer shielding factor R_{5d} for the 5*d* electron.

ACKNOWLEDGMENTS

We would like to thank Dr. L. S. Goodman for much of the design of the apparatus, construction of the rf section, and many helpful discussions during this work. We also thank Mr. E. Hohman, Mr. C. Kurtz, and Dr. U. Nielsen for their assistance during the construction of the apparatus. This research was supported by the U.S. Department of Energy, Office of Basic Energy Sciences, under Contract No. W-31-109-Eng-38.

[1] I. I. Rabi, J. R. Zacharias, S. Millman, and P. Kusch, Phys. Rev. **53**, 318 (1938).
[2] J. Brossel and A. Kastler, C. R. Acad. Sci. **229**, 1213 (1949).
[3] S. D. Rosner, R. A. Holt, and T. D. Gaily, Phys. Rev. Lett. **35**, 785 (1975).
[4] S. D. Rosner, T. D. Gaily, and R. A. Holt, Phys. Rev. Lett. **40**, 851 (1978).
[5] U. Nielsen, O. Poulsen, P. Thorsen, and H. Crosswhite, Phys. Rev. Lett. **51**, 1749 (1983).
[6] M. Van Hove, G. Borghs, P. de Bisschop, and R. E. Silverans, Z. Phys. A **321**, 215 (1983).
[7] T. J. Scholl, T. D. Gaily, R. A. Holt, and S. D. Rosner, Phys. Rev. A **33**, 2396 (1986).
[8] U. Nielsen, K. T. Cheng, H. Ludvigsen, and J. N. Xiao, Phys. Scr. **34**, 776 (1986).
[9] A. Sen, L. S. Goodman, W. J. Childs, and C. Kurtz, Phys. Rev. A **35**, 3145 (1987).
[10] K. Krebs and R. Winkler, Z. Phys. **160**, 310 (1960).
[11] R. Winkler, Phys. Lett. **16** 156 (1965).
[12] G. Guthörlein, Z. Phys. **214**, 332 (1968).
[13] A. Arnesen, A. Bengtson, R. Hallin, C. Nordling, Ö. Staaf, and L. Ward, Phys. Scr. **24**, 7474 (1981).
[14] K. Dörschel, W. Heddrich, H. Hühnermann, E. W. Peau, and W. Wagner, Z. Phys. A **312**, 269 (1983).
[15] S. L. Kaufman, Opt. Commun. **17** 309 (1976).
[16] W. H. Wing, G. A. Ruff, W. E. Lamb, and J. J. Spezeski, Phys. Rev. Lett. **36**, 1488 (1976).
[17] H. J. Andrä, in *Beam-foil Spectroscopy,* edited by J. A. Sellin and D. J. Pegg (Plenum, New York, 1976), Vol. 2, p. 835.
[18] *Handbook, Tri-Plate Microwave Components,* edited by R. W. Peters (Sanders, Nashua, NH, 1956), p. 8. The design of the rf section is by L. S. Goodman.
[19] See, e.g., I. Lindgren and J. Morrison, in *Atomic Many-Body Theory* (Springer, Berlin, 1983), Chap. 14.
[20] I. Lindgren, Rep. Prog. Phys. **47**, 345 (1984).
[21] C. Schwartz, Phys. Rev. **97**, 380 (1955).
[22] P. G. H. Sandars and J. Beck, Proc. R. Soc. London, Ser. A **289**, 97 (1965).
[23] I. Lindgren and A. Rosen, Case Stud. At. Phys. **4**, 93 (1974); **4**, 197 (1974).
[24] L. Armstrong, Jr., *Theory of Hyperfine Structure of Free Atoms* (Wiley-Interscience, New York, 1971).
[25] *Atomic Energy Levels,* edited by W. C. Martin, R. Zalubas and L. Hagan, Natl. Bur. Stand. Ref. Data Ser., Natl. Bur.

Stand. (U.S.) Circ. No. 60 (U.S. GPO, Washingtion, D.C. 1978).
[26]W. J. Childs, Phys. Rev. A **2**, 316 (1970).
[27]L. Evans, P. G. H. Sandars, and G. K. Woodgate, Proc. R. Soc. London, Ser. A **289**, 114 (1965).
[28]Y. Tanaka, R. M. Steffen, E. B. Shera, W. Reuter, M. V. Hoehn, and J. D. Zumbro, Phys. Rev. Lett. **51** 1633 (1983).
[29]R. A. Carrigan, Jr., P. D. Gupta, R. B. Sutton, M. N. Suzuki, A. C. Thomson, R. E. Coté, W. V. Prestwich, A. K. Gaigalas, and S. Raboy, Phys. Rev. Lett. **20**, 874 (1968).
[30]R. M. Sternheimer, Phys. Rev. **146**, 140 (1966); **164**, 10 (1967).
[31]W. J. Childs and K. T. Cheng, Phys. Rev. A **30**, 677 (1984).
[32]H. Brand, V. Pfeufer, and A. Steudel, Z. Phys. A **302**, 291 (1981).
[33]K. Dörschel, W. Heddrich, H. Hühnermann, E. W. Beau, H. Wagner, G. D. Alkhazov, E. Ye. Berlovich, V. P. Denison, V. N. Panteleev, and A. G. Polyakov, Z. Phys. A **317**, 233 (1984).
[34]S. A. Ahmad, W. Klempt, C. Ekström, R. Neugart, and K. Wendt, Z. Phys. A **321**, 35 (1985).
[35]K. E. G. Löbner, M. Vetter, and V. Hönig, Nucl. Data Tables A **7**, 495 (1970).
[36]R. M. Sternheimer (private communications), as quoted in H.-P. Clievers *et al.*, Z. Phys. A **289**, 361 (1979).
[37]U. Nielsen (private communication).